Mass acquisition of Dirac fermions in magnetically doped topological insulator Sb_2Te_3 films

Yeping Jiang,[1,2] Canli Song,[1,3] Zhi Li,[4] Mu Chen,[1] Richard L. Greene,[2] Ke He,[1,3] Lili Wang,[1,3] Xi Chen,[1,3] Xucun Ma,[1,3,4,*] and Qi-Kun Xue[1,3,†]

[1]*State Key Laboratory of Low-Dimensional Quantum Physics, Department of Physics, Tsinghua University, Beijing 100084, People's Republic of China*

[2]*Center for Nanophysics and Advanced Materials, Department of Physics, University of Maryland, College Park, Maryland 20742, USA*

[3]*Collaborative Innovation Center of Quantum Matter, Beijing 100084, China*

[4]*Institute of Physics, Chinese Academy of Sciences, Beijing 100190, People's Republic of China*

(Received 22 January 2015; revised manuscript received 10 September 2015; published 18 November 2015)

We report on the mass acquisition of Dirac fermions by doping Cr into the topmost quintuple layer or into the bulk of Sb_2Te_3 topological insulator films. By careful investigation of the scanning tunneling microscopy/spectroscopy on the films, we find that the Landau level spectrum keeps a good quality even at a high Cr-doping level, enabling a demonstration of deviation of the zeroth Landau level, induced by the acquisition of a mass term in the surface states in the presence of surface or bulk magnetic doping. The magnitude of the mass term in the surface states increases with increasing Cr-doping level. Our observation suggests Cr-doped Sb_2Te_3 is a promising candidate for the realization of the proposed magnetoelectric effects.

DOI: 10.1103/PhysRevB.92.195418 PACS number(s): 71.70.Di, 68.37.Ef, 73.20.At, 75.70.−i

I. INTRODUCTION

Three–dimensional (3D) strong topological insulators (TIs), since their discovery, have attracted tremendous research interests due to the topologically nontrivial gapped bulk band and the existence of gapless Dirac fermion surface states [1,2], which are protected by time-reversal symmetry (TRS). The gapless nature of topological surface states can be broken by introducing perturbations such as magnetic ordering, which may change the system into a gapped two-dimensional (2D) Dirac fermion system and make inductions of novel topological magnetoelectric response (TME) [3–6]. For example, quantum anomalous Hall effect has been proposed and experimentally realized in ferromagnetic TI films in the 2D limit [7,8].

So far the most studied three-dimensional TI systems are Bi_2Se_3, Bi_2Te_3, and Sb_2Te_3, which have a single Dirac cone in their surface state electronic structures within a relatively large bulk gap [9–11]. Ways to introduce TRS breaking includes surface or bulk magnetic doping [12–15], and by proximity to ferromagnetic materials [5]. One drawback of the doping approach is that the bulk doping of lighter magnetic elements will decrease the spin-orbit coupling strength and may eventually eliminate the nontrivial bulk band topology, which, fortunately, as demonstrated in a recent work [16] and also here, is quite robust and can persist at a relatively high magnetic doping level. Ferromagnetism does emerge in TIs with bulk magnetic doping [17,18]. A lot of efforts have been reported in evidencing a massive gap of various origins [18–32]. Scanning tunneling microscopy (STM)-based Landau level (LL) spectroscopy has been shown to be a powerful local tool to investigate the dispersion of topological surface states [27,33–36]. Here we use LL spectroscopy as a mass-term sensitive probe to investigate the mass acquisition phenomena in topological surface states of Cr-doped Sb_2Te_3 films. We show that, both in surface- and bulk-doped samples, the zeroth LL, which has been taken as a unique signature of Dirac fermions, will deviate from the Dirac energy, indicative of a mass acquisition.

II. METHODS

A. Mass term acquisition and Landau level formation in the presence of magnetic doping and the perpendicular magnetic field

By introducing magnetic dopants, the Dirac Hamiltonian of topological surface states is $H = -\mu I + \hbar v_F(k_x\sigma_2 - k_y\sigma_1) + m\sigma_3$, where a mass m comes into play because of the exchange interaction between magnetic dopants and surface state electrons: $H_{\rm ex} = -J\sum \mathbf{S}_i\cdot\mathbf{s}\delta(\mathbf{r}-\mathbf{R}_i)$. By only taking the effect of the z-component spin (perpendicular direction) of dopants, $H_{\rm ex}|_z = -Jn_{\rm Cr}\bar{S}_z\sigma_3/2$. Here μ is the chemical potential relative to the charge neutrality point (Dirac point $E_D = -\mu$), σ_i are spin Pauli matrices, $\bar{S}_z$ is the z component of averaged dopant spin, and $n_{\rm Cr}$ is two-dimensional doping density. Thus, $m = -\frac{1}{2}Jn_{\rm Cr}\bar{S}_z = -JM_z/2\mu_B$, where M_z is the local magnetization in the z direction. The in-plane spin components, though also being TRS-breaking terms, only shift the Dirac point in the equi-energy plane in momentum space, and are not included here. The resulting surface state dispersion is $E_\pm = -\mu \pm\sqrt{\hbar^2v_F^2k^2 + m^2}$, with a gap of $2m$ in the surface states.

In the presence of a perpendicular magnetic field, Landau levels form in the surface state spectrum. The Hamiltonian in the field simply becomes $H = -\mu I + \hbar v_F(k'_x\sigma_2 - k'_y\sigma_1) + (m + \frac{1}{2}g_s\mu_B B)\sigma_3$, taking into account the effect of magnetic field by adding the magnetic vector potential to the momentum operator $\hbar\mathbf{k}' = \hbar\mathbf{k} + e\mathbf{A}$ and adding the Zeeman term $\frac{1}{2}g_s\mu_B B\sigma_3$, where g_s is the g factor of surface state electrons. Similar to the exchange term, in the Zeeman term $H_z = g_s\mu_B\hbar^{-1}\mathbf{B}\cdot\mathbf{s}$, only a perpendicular magnetic field will add a mass term to the surface states. The Hamiltonian reads

$$H = \begin{pmatrix} -\mu + \Delta & iv_F\sqrt{2e\hbar|B|}a \\ -iv_F\sqrt{2e\hbar|B|}a^\dagger & -\mu - \Delta \end{pmatrix} \quad (1)$$

*Corresponding author: xucunma@mail.tsinghua.edu.cn
†Corresponding author: qkxue@mail.tsinghua.edu.cn

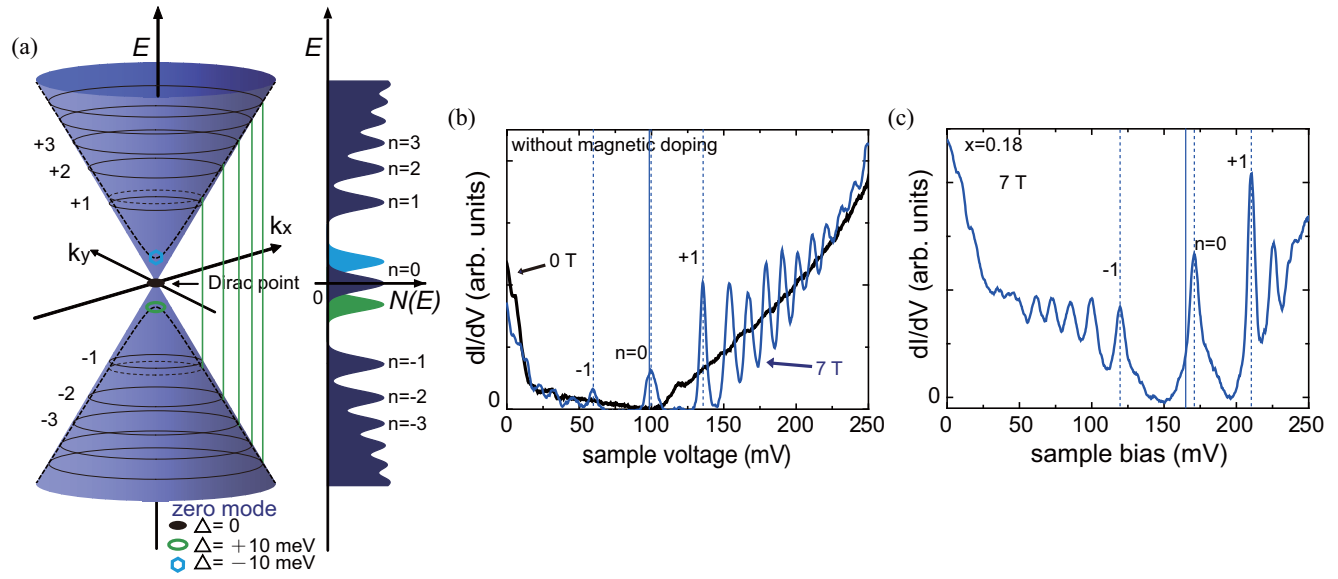

FIG. 1. (Color online) (a) Schematic of surface states of a 3D TI and the Landau quantization scheme with and without massive gap neglecting the field induced Zeeman term. The sign of zero-mode deviation depends on the sign of TRS-breaking mass terms of $\Delta = 0$, ± 10 meV. (b) The STS on an Sb_2Te_3 film (sample 2 without Cr doping) at 0 and 7 T. (c) The STS on the Sb_2Te_3 film with surface Cr doping of $x = 0.18$ (sample 2). The dashed lines indicate Landau levels of $n = -1, 0, +1$, while the solid line is the midpoint energy of $n = \pm 1$ Landau levels. Tunneling gap conditions: $V_{\text{bias}} = 0.2\,\text{V}$, $I = 200\,\text{pA}$.

by introducing the creation and annihilation operators $a^\dagger$ and a as linear combinations of k'_x and k'_y such that $[a, a^\dagger] = 1$. This simple eigenstates problem can be easily solved by defining the eigenstates $\varphi_n = \binom{c_1|n-1\rangle}{c_2|n\rangle}$, where $|n\rangle$ are the eigenvectors of the number operator $a^\dagger a$. The Landau level energies except for the zeroth mode are given by

$$E_n = E_D \pm \sqrt{2e\hbar v_F^2 B|n| + \Delta^2}, \quad n = \pm 1, \pm 2, \ldots, \qquad (2)$$

where $\Delta = JM_z/2\mu_B + \frac{1}{2}g_s\mu_B B$ is the mass term. The energy of zero-mode LL is

$$E_0 = E_D - \text{sgn}(B)JM_z/2\mu_B - \tfrac{1}{2}g_s\mu_B|B|. \qquad (3)$$

Here we have $\varphi_0 = \binom{0}{|0\rangle}$, indicating that the zeroth LL is very special since it is fully spin polarized.

This form of energy quantization [Eq. (2)] means that, in the massive Dirac fermion system, the phase offset γ in the Onsager quantization relation $S(E_n) = \pi k_n^2 = \pi(E_n^2 - \Delta^2)/\hbar^2 v_F^2 = 2\pi eB[n + \gamma]/\hbar$ is exactly zero, duplicating the massless case [Fig. 1(a)], such as graphene and TRS-preserved TIs, where the half-integer quantization is due to the Berry phase of π [37]. In general, the quantization condition changes with Berry phase. For an ordinary electron system with parabolic dispersion and Berry phase of 0, $\gamma = \frac{1}{2}$ [38], leading to integer quantization. For gapped Dirac fermions, induced by TRS breaking or tunneling between two copies of surface states in TIs [27,32], or by sublattice symmetry-breaking mechanism in the graphene case, where the Berry phase deviates from π with the form $\Phi = \pi(1 - \frac{\Delta}{E})$ [5,39], $\gamma = 0$ still holds. The quantum oscillation measurement, which measures γ, cannot tell if there is a mass Δ in a Dirac electron system, except for an addition of the particle-hole breaking term $\hbar^2 k^2/2m_e^*$ [40]. This term here is neglected due to the nearly idea linear dispersion of surface states in Sb_2Te_3 films compared with Bi_2Se_3 [27].

The energy of zero-mode LL [Eq. (3)], which is the central issue of our work, deviates from the Dirac energy E_D due to the mass term Δ, as shown in Fig. 1(a). From Eq. (2) we can define the E_D by the midpoint (MP) energy between ± 1 LLs, which are symmetric with respect to E_D. The sign of the Zeeman term in the mass term $\Delta = JM_z/2\mu_B + \frac{1}{2}g_s\mu_B B$ only depends on the sign of g factor. For Sb_2Te_3 films without magnetic doping, there is nearly no discernible deviation with all the zeroth LLs measured fluctuating around E_D in the range of -1 to $+1$ meV at 7 T, giving an upbound $g_s \approx 5$, which is relatively small and may be quite different from the bulk value. As can be seen in the experimental scanning tunneling spectrum (STS) of an Sb_2Te_3 thin film without Cr doping in Fig. 1(b), the zeroth LL position is symmetric relative to ± 1 LL energies and nearly coincides with the energy of the state with zero density of states (DOS) at zero fields. Thus, here we only consider the mass term induced by Cr doping. Hence, the deviation only depends on the term $-\Delta = -\text{sgn}(B)JM_z/2\mu_B$, with the sign determined by the sign of exchange coupling J, the relative direction between the magnetization and the magnetic field. In real materials, MP $(-n, +n)$ does not coincide with the Dirac energy in the undoped case because of the existence of a high order correction term in Fermi velocity [41]. Here we choose MP $(-1, +1)$ as the measure of the Dirac energy to determine the possible mass term in the magnetically doped materials where the zeroth LL no longer coincides with the Dirac energy. As shown in the measured spectra in the undoped case, MP $(-1, +1)$ coincides nearly perfectly with the zeroth LL because the high order correction can be neglected at low momentum k.

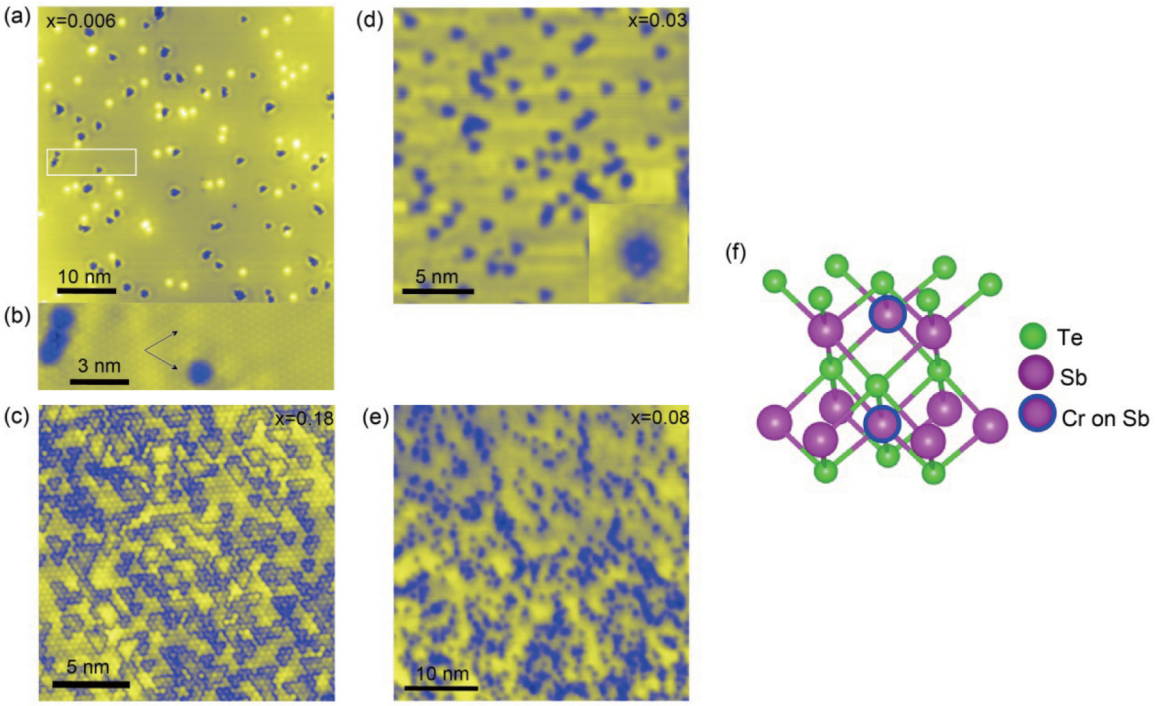

FIG. 2. (Color online) (a) STM image (−1.0 V, 50 pA) of Sb_2Te_3 film with surface Cr doping (sample 1, $x = 0.006$). (b) Zoom-in high-resolution image (0.1 V, 40 pA) in (a), showing Cr_{Sb1} defects after surface Cr doping. (c) High resolution STM image (0.2 V, 400 pA) of Sb_2Te_3 film with surface Cr doping (sample 2, $x = 0.18$). (d) STM image (−1.0 V, 200 pA) of Sb_2Te_3 film with bulk Cr doping ($x = 0.03$). The inset in (d) shows the atomic resolution image of dark dots induced by Cr doping. (e) STM image (1.0 V, 50 pA) of Sb_2Te_3 film with bulk Cr doping ($x = 0.08$). (f) Schematic of surface Cr doping and the atomic structure of 1 QL Sb_2Te_3, showing Cr on Sb1 (first Sb layer from the surface).

B. Experiment

All experiments were carried out in an ultrahigh-vacuum system, equipped with a molecular beam epitaxy (MBE) chamber and a low temperature STM having a 7 T magnet. The base pressure of the system is better than 1×10^{-10} Torr. In the MBE growth of Sb_2Te_3 films, highly n-doped and graphitized 6H-SiC (0001) covered mainly by bilayer graphene was used as the substrate. Sb_2Te_3 films were prepared by thermal evaporation of high-purity Sb (99.9999%) and Te (99.9999%) from two standard Knudsen cells. During growth, the temperatures of the Sb source, the Te source, and the substrate were set at around 330, 225, and 230 °C, respectively, resulting in a growth rate of about 0.2 QL/min and a Te/Sb flux ratio of about 10. High-purity Cr atoms (99.999%) were evaporated from a tantalum boat by electric current heating (∼1000 °C). By varying the growth conditions, a high quality of Sb_2Te_3 films with different intrinsic defect levels can be obtained. In this study, the bulk Cr-doped samples (film thickness $d \sim$ 50 quintuple layers (QL), the Dirac energy $E_D \sim 160$, and 180 meV for Cr-doping levels of 0.03 and 0.08) were prepared by co-deposition of Sb, Te, and Cr [Figs. 2(d) and 2(e)]. As for samples with surface Cr doping, we first prepared pure Sb_2Te_3 films with different intrinsic doping (samples 1 and 2, $d \sim$50 QL and $E_D \sim 100$ meV; sample 3, $d \sim$ 40 QL and $E_D \sim 75$ meV). Then, Cr was deposited on the Sb_2Te_3 surface at low temperature (100 K), following an annealing process at 200 °C for hours [Figs. 2(a)–2(c)]. For films without Cr doping, above certain thickness (∼10 QLs), it is the intrinsic defect concentration that controls the Dirac energy, not the thickness. The dependence of Dirac energy on thickness, which comes from substrate transfer doping, can be neglected above 10 QLs [42]. The samples with bulk Cr doping are labeled as $(Sb_{1-x}Cr_x)_2Te_3$. For samples with surface Cr doping, x denotes the ratio between Cr doping in the first QL and surface atom density. The relatively low annealing temperature does not introduce extra defects other than substituting Cr into the lattice. Moreover, a stepwise strategy, with a maximum doping of $x = 0.03$ in each step, was used to avoid Cr-cluster formation. The nominal Cr-doping levels range from 0.006 to 0.21.

All STM data was taken at 4.8 K. Prior to the STM/STS measurements, a polycrystalline W tip is cleaned by electron-beam heating in an MBE chamber, and then calibrated with Ag/Si(111) films. All the differential conductance spectra and maps are acquired using a standard lock-in technique with a bias modulation of 1 mV at 987.5 Hz. The bias voltage was applied to the sample. The LL curves shown in this work are all single point spectra except Figs. 6(a) and 6(b) for bulk-doped samples.y

III. RESULTS AND DISCUSSIONS

We then investigate the effect of surface or bulk Cr doping on the topological surface states by LL spectroscopy. First, the morphology of Sb_2Te_3 films with surface and bulk Cr doping were well characterized by STM. Figures 2(a) and 2(c)

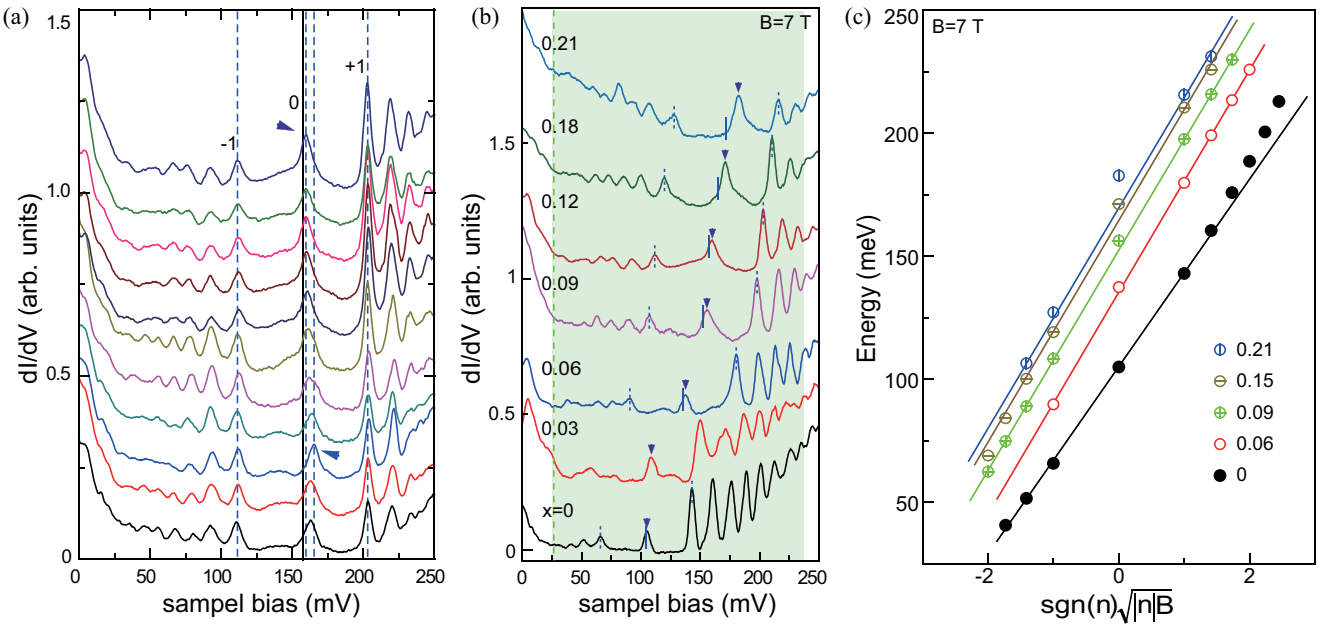

FIG. 3. (Color online) (a) LL spectra taken at random positions on sample 2 at $x = 0.12$, showing the spatial variation of zero-mode deviation (2.4–7.2 meV). The arrows indicate the zeroth LLs coinciding with the dashed lines. The solid line and dashed lines around the zeroth LL indicate the Dirac energy and the range of zero-mode deviations, respectively. We see that the zeroth LL always deviates in the positive directions. (b) STS at 7 T (0.2 V, 200 pA) on sample 2 with increasing Cr doping x: 0, 0.03, 0.06, 0.09, 0.12, 0.18, 0.21. The arrows indicate the zeroth LLs. The dashed short lines indicate the ± 1 LLs, while the solid short ones indicate the Dirac energies. Spectra of different doping are shifted vertically for clarity. (c) LL energies were plotted against $\mathrm{sgn}(n)\sqrt{|n|}$ at various Cr-doping levels in sample 2. The linear fitting to the data except for zeroth LL gives a Fermi velocity of 4.8×10^{-5} m/s for the Cr-doped case.

show the STM images of Sb_2Te_3 film with different surface Cr-doping levels. The bright spots are intrinsic Sb_{Te} (Sb on Te) defects in the topmost Te layer [42]. We find that Cr atoms exclusively substitute for Sb atoms probably due to the large difference in ion sizes between Cr and Te atoms. The dark triangle spot [Fig. 2(b)] correspond to Cr_{Sb1} defects, due to the suppressed electronic states on three surface Te atoms adjacent to the substitutional Cr atom in first Sb lattice (Sb1) from the surface [Figs. 2(b) and 2(f)]. The surface deposition and annealing procedure only introduces Cr_{Sb1} demonstrated by the similarity between the number of surface Cr ad-atoms before annealing and that of Cr_{Sb1} defects after annealing. Even at a high doping level [$x = 0.18$, Fig. 2(c)], the Cr atoms still only substitute into the first Sb layer and the topmost Te layer keeps well ordered and clean. Here top-Sb-layer Cr doping means the Cr doping into the first Sb layer. The same defect structure is observed in the samples with bulk Cr doping [Figs. 2(d) and 2(e)]. Certainly the doping of light element such as Cr will change the lattice constant. However, the Cr doping in Sb_2Te_3 does not induce disorders such as clusters that will destroy the layered structure of the film. The preserved crystalline lattice, the clean surface, the isovalent, and uniform nature of doping, all together make it possible for the LL spectra to keep a good quality and enable the possibility of observing the zero-mode behavior by, other than introducing a mass term to the surface states, not inducing considerable scattering events.

First we focus on the Cr doping into the first quintuple layer of Sb_2Te_3 films grown by MBE. Note that all Sb_2Te_3 films are hole doped due to the intrinsic p-type defects [42]. In this study, samples 1 and 2 have similar Dirac energy ($E_D \sim 100$ meV) at zero Cr doping, while sample 3 has a lower intrinsic hole doping ($E_D \sim 75$ meV). Then the three samples are surface doped by Cr atoms stepwise up to 0.105, 0.21, and 0.18, respectively. Among them, sample 2 is more thoroughly investigated, with spectra at all different Cr doping levels taken step wisely. Figure 1(c) shows a corresponding LL spectrum taken on the film (sample 2) with $x = 0.18$, where a series of well-defined LL peaks can be seen. Compared with the undoped case [$x = 0$, Fig. 1(b)], where the TI surface states are expected massless [27], the well separated zeroth LL is no longer symmetric relative to the positions of ± 1 LLs, shifting positively with a magnitude of about 6 meV from the Dirac energy, implying the existence of a mass term. We assume that at a high magnetic field of 7 T, the z components of magnetic moments align with the magnetic field in the same direction. The positive deviation (negative mass term Δ) implies a negative exchange interaction J between the spin of surface state electrons and that of the Cr dopants. The mass term for films with surface Cr doping is spatially inhomogeneous as indicated in Fig. 3(a), where the LL spectra were taken at random positions on sample 2 ($x = 0.12$). The zeroth LLs at different positions deviate positively from E_D by the value of 2.4–7.2 meV, while the higher LL energies keep uniform implying the homogeneity of charge doping. From the varying zeroth LL positions and the unvarying ± 1 LLs, we can see clearly the irrelevance between variation in the zeroth LL deviation and charge doping. The homogeneity of charge doping can also be suggested by the absence of LL splitting in our measurement [43]. Actually, in films with Sb

vacancies which induce a high potential variation spatially, we do observe LL splitting frequently. The spatial inhomogeneity of the mass term is due to the spatial variation of Cr doping.

The mass term increases with increasing Cr-doping levels as shown in Figs. 3(b) and 3(c). Δ increases from 0 at zero Cr doping to about 12 meV at $x = 0.21$. Besides the zero-mode deviation, the Cr doping lifts up the Dirac energy. The Dirac energy moves steadily upwards, from around 100 meV without doping to around 170 meV in the heavily doped case ($x = 0.21$). This is not caused by a carrier-doping effect. The Fermi level is nearly unchanged relative to the bulklike valence band edge (dashed line), which is consistent with the literature [44]. We observed a similar behavior in the bulk Cr-doping case [Figs. 6(a) and 6(b)], ruling out the possibility of surface band bending due to this top-Sb-layer Cr doping. This is a rigid band shift between the surface Dirac cone and the bulklike band, supported by the increasing or decreasing number of LLs below or above the Dirac energy. The shaded region, which does not change with Cr doping, is roughly the bulk gap where LLs emerge. While the existence of Dirac point (Kramer degenerate point) is guaranteed by TRS, its energy varies in different materials. This is consistent with what has been calculated and observed in Sb-doped Bi_2Te_3, where the bulk doping of elements (Sb) having smaller spin-orbit coupling strength lifts the Dirac energy and decreases the Fermi velocity [45,46]. Theoretically, the Dirac cone can be also engineered by changing the elements in the topmost atomic layer [47]. We see here similar behavior in both cases of bulk and top-layer Cr doping.

From the aforementioned Onsager quantization condition $k_n^2 = 2\frac{e}{\hbar}|n|B$ and Eq. (2), the dispersion of gapped surface states can be simulated by taking field dependent LL spectra. In Fig. 4 we show the data in three samples with different Cr-doping levels: sample 1 ($x = 0.105$), sample 3 ($x = 0.18$), and sample 2 ($x = 0.21$). The LL energies except the zeroth one keep a good linearity, just like the case without Cr doping because Eq. (1) indicates that the deviation for LLs with higher $|n|B$ from the gapless case is nearly indiscernible (less than 0.5 meV for $\Delta = 5$ meV and lowest available $|n|B$: $n = 1$, $B = 3$ T). For films with Cr-doping levels, the zeroth LL deviation is nearly constant above the magnetic field at which it becomes discernible [see Fig. 4(a)], implying a low saturation field of ≤ 1 T for magnetization of dopants in the first QL. The fitting of the data to Eq. (2) is quite good [Fig. 4(c)], showing a massive Dirac dispersion. The field dependent data are similar for the film with even higher Cr doping ($x = 0.21$), which exhibits a relatively larger massive gap as shown in Fig. 4(d).

In addition, at such high doping of Cr ($x = 0.21$), the first QL is still found to be topologically nontrivial, considering Cr is less than half of Sb in the atomic mass. We demonstrate it by growing submonolayer epitaxial Sb_2Te_3 film on top of sample 3 of $x = 0.18$, resulting in a $Sb_2Te_3/(Sb_{1-x}Cr_x)_2Te_3/Sb_2Te_3$ sandwich structure in the perpendicular direction [Figs. 5(a) and 5(c)]. Figure 5(a) shows three terraces. On the second terrace we show the atomic resolution image [Fig. 5(b)] of the interface region between doped and undoped Sb_2Te_3. The interface is epitaxial. On the undoped region, below which there is a doped layer, a *dI/dV* image at the energy of zeroth LL (135 meV) was taken. The absence of LLs in some region [curve 4 or the dark region in Fig. 5(d)] may be due to the lattice mismatch between the undoped layer and the doped layer underneath. Here we also observe a shift of Dirac energy on the undoped region before and after applying a magnetic field (curve 0 and the dispersion of curve 2), which is not clearly understood. Because of the van der Waals nature between quintuple layers the induced strain by Cr doping should be negligible. The lattice mismatch itself may have considerable effect on the electronic state overlap between TI quintuple layers. In addition, the strain in the doped Sb layer underneath is not homogeneous, resulting in a nonperiodic pattern of lattice mismatch. Another work [48] reveals that the Ag intercalation between first and second QLs increases the van der Waals gaps. As a result, the first QL becomes somewhat isolated and the topological surface states are pushed to the second QL. In the case of Sb_2Te_3, one completely isolated QL behaves like a 2D trivial insulator, with a much larger gap of about 650 meV [27]. The underlying irregular lattice mismatch pattern could possibly explain the spatially inhomogeneous surface state spectral intensity. Another proof supporting the preserved nontrivial surface states in the undoped overlayer

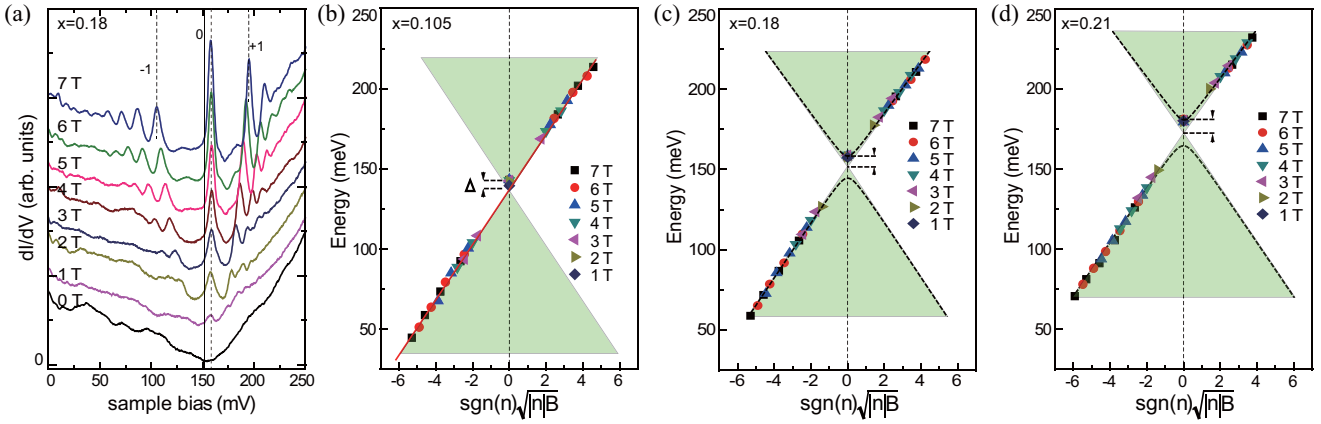

FIG. 4. (Color online) (a) Field dependent LL spectra (0.2 V, 200 pA) on sample 3 ($x = 0.18$). The solid line indicates the Dirac energy. (b)–(d) LL energies under various magnetic fields plotted versus $\mathrm{sgn}(n)\sqrt{|n|B}$ on samples of $x = 0.105$ (sample 1), 0.18 (sample 3), 0.21 (sample 2), respectively. The red line in (b) is a linear fitting to the date except the zeroth LL. The dashed curves in (c) and (d) are the fitting according to the quantization condition $E_n = \mathrm{sgn}(n)\sqrt{2e\hbar v_F^2 B|n| + \Delta^2}$ of the gapped surface states.

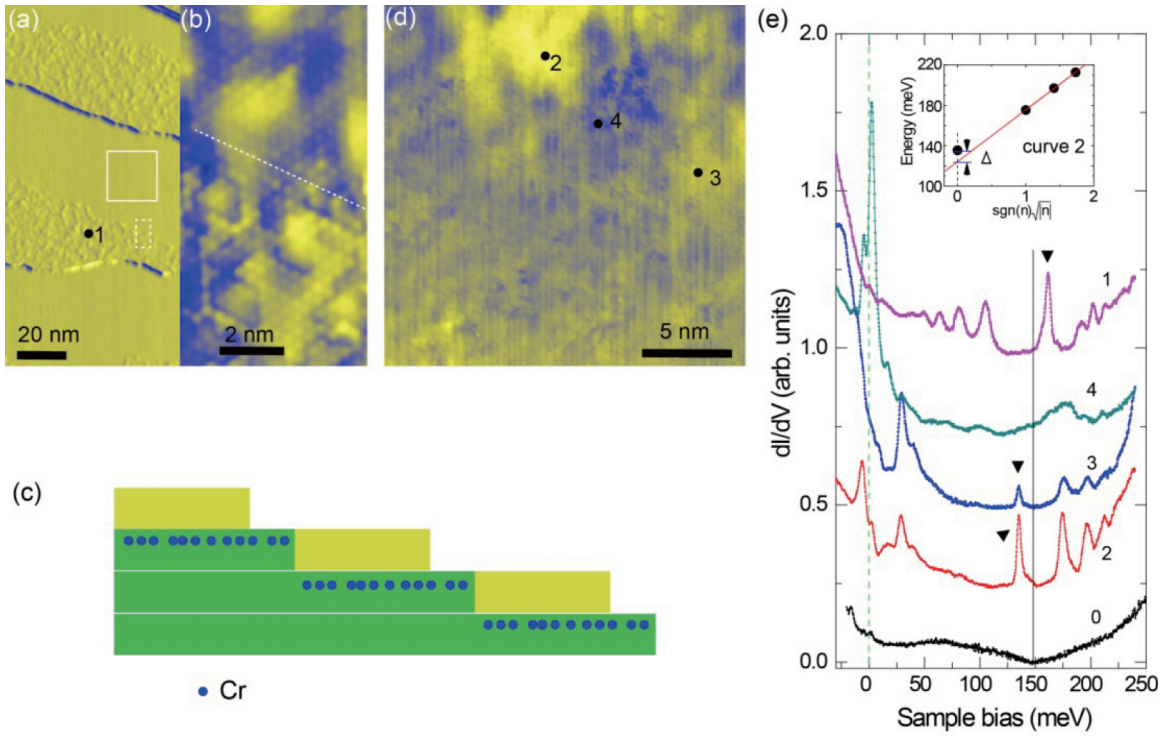

FIG. 5. (Color online) (a) STM image (derivative) of epitaxial Sb_2Te_3 film grown on sample 3 ($x = 0.18$). (b) The atomic resolution image of the boundary between doped and undoped region indicated by a dashed rectangle in (a). (c) Schematic of the heterostructure. (d) *dI*/*dV* mapping of the squared region in (a) at 135 mV, where the zeroth Landau level appears in the surface state spectra at 7 T. (e) Spectra 1–4 are taken at corresponding positions indicated in (a) and (d) at 7 T. Spectrum 0 is a typical one taken in the squared region at zero magnetic field. The inset shows the dispersion of spectrum 2. The triangle arrow indicates the zeroth LL.

is that the magnitude of zeroth-LL deviation [the inset in Fig. 5(e)] is similar to that on the doped layer. This implies a common origin of zeroth-LL deviation. Thus the existence of LLs with Dirac dispersion on the newly grown monolayer film without doping suggests the persistence of nontrivial band topology in the system with Cr doping of 0.18.

Remembering that the sign of the mass term depends on the relative direction between the magnetization and magnetic field [49], the zero mode may flip from above E_D to below E_D by flipping the magnetic field into opposite direction but with a magnitude smaller than the coercive field of possible ferromagnetism in the top-Sb-layer doping case. We measured the surface state spectra by changing the magnetic field in small steps around zero (not shown). The zero-mode flipping or the hysteresis behavior was not observed. Actually, in order to see this behavior, a coercive field of around 1 T is needed (zeroth LL does not appear below 1 T), while for this material it is only about 0.1 T [44]. Thus, the zero-field mass term or ferromagnetism in the top-Sb-layer doping case remains open for further study.

Although we have excluded some trivial effects that would cause the deviation of zeroth LL, the induced strain by Cr doping may also change the surface states [50,51]. For example, the surface state dispersion may be changed, resulting in different Fermi velocities below and above the Dirac energy. But this effect is relatively small and less likely the cause of the zeroth LL deviation. It cannot explain the large deviation of zeroth LL as shown in Fig. 3(c) for the highest doping level of $x = 0.21$ in the first-Sb-layer doping case or as shown in Fig. 6(a) for the bulk doping case. The comparison between a magnetically and nonmagnetically doped (dopants with similar atomic size but with or without magnetic moments) sample would be a possible evidence [18].

In our experiment we did another comparison experiment which could possibly support the time-reversal-symmetry-broken scenario of zeroth LL deviation. For comparison, we discuss the bulk Cr-doping case. Figures 6(a) and 6(b) show the spectra taken on two films with bulk Cr doping of $x = 0.03$ and 0.08. For the film of $x = 0.03$, the zero field spectrum shows no anomalous behavior, similar to the massless case probably because of the absence of ferromagnetism at 4.8 K in the low Cr-doping case. In the magnetic field of 7 T, the aligned magnetic moments introduce a mass term. The zeroth LL deviates by about 11 meV from the Dirac energy defined by the mid energy of ± 1 LLs and from the energy where the DOS is approximately zero at zero magnetic field. The zero-DOS energy at 0 T nearly coincides with E_D. This phenomenon is more explicitly shown by the deviation of zeroth LL from linearity in the inset. Things are somehow different for the $x = 0.08$ case. At zero magnetic field there is a prominent enhancement near E_D in the surface state DOS, which may be ascribed to the impurity induced states [52]. In some region on the film, the spectrum even shows a fully gaped feature (data not shown). Thus, compared with the top-Sb-layer doping case, the bulk doping also lifts the Dirac energy and introduces a mass term, but with a much larger magnitude. The Dirac energies shift to approximately 160 and 180 meV for $x = 0.03$

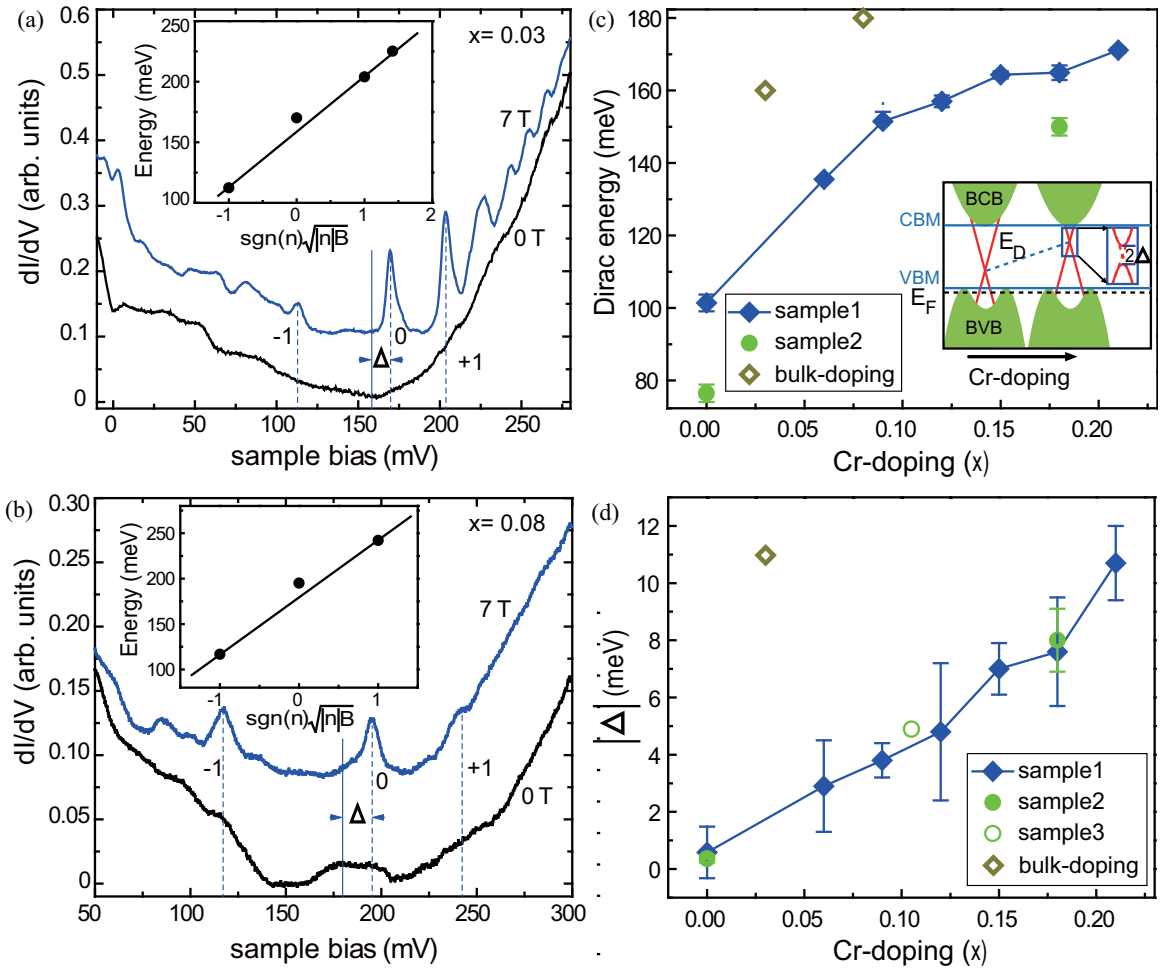

FIG. 6. (Color online) (a) and (b) Spatial averaged zero-field STS and LL spectra [0.2 V, 200 pA for (a); 0.25 V, 200 pA for (b)] taken at random positions on the $(Sb_{1-x}Cr_x)_2Te_3$ films with bulk Cr doping ($x = 0.03$ and 0.08). The LL spectra are shifted vertically for clarity. The insets are the surface state dispersion derived from the LL spectra. The lines are the linear fitting to the Landau levels except the zeroth ones. The +1 LL in (b) is barely resolved because it becomes quite close to the bulklike conduction band edge due to the lifted Dirac energy. (c) and (d) Doping dependence of Dirac energy E_D and the mass term Δ. The inset shows the schematic of the effect of Cr doping on the surface state structure. Here E_D indicates Dirac energy of surface states, which can be obtained from the ± 1 LL energies. CBM and VBM indicate the band edge of bulklike conduction band (BCB) and valence band (BVB).

and 0.08, with the corresponding mass terms Δ at 7 T of around 11 and 16 meV, respectively. For top-Sb-layer doping of $x = 0.08$, Δ is about 4 meV, about four times smaller in magnitude than that of bulk doping. It is understandable considering that in our top-Sb-layer doping scheme Cr atoms only substitute the first Sb layer. Based on the observation that the critical thickness for Sb_2Te_3 being a three-dimensional TI is around 4 QL, the surface state electrons are supposed to have a spatial extension of about 2 QLs, implying that the Dirac fermions may have interaction with the dopants' spins in the first four Sb atomic layers. In addition, we find a high homogeneity in the spatial distribution of the mass term, in contrast to the top-Sb-layer doping case, probably due to a more uniform overall Cr-doping level in 2 QLs than that doped only in the first Sb layer. This is where the error bars for top-Sb-layer doping in Figs. 6(c) and 6(d) come from. The fact that the magnitude of zeroth-LL deviation in the bulk-doped sample is almost four times that in the top-Sb-layer doped sample with the same doping ratio in one Sb layer and that this deviation scales with doping levels are consistent with the magnetic doping scheme and cannot be explained by the lattice-constant change or strain scheme. In the latter scheme, the two doping method with the same doping ratio in the individual Sb layer should have the same lattice distortion.

Figures 6(c) and 6(d) display a summary of Cr-doping effect on the topological surface states in Sb_2Te_3 films. First, the Dirac cone shifts rigidly upwards relative to the bulklike band. As illustrated by the schematic in the inset of Fig. 6(c), the doping dependent Dirac energy for two different intrinsic doped samples shows the upward shift in E_D of about 70 meV at $x = 0.21$. The offset in energy between the two data sets for sample 2 and sample 3 originates from different Fermi energies, which does not change much with the increasing Cr doping. Second, the mass term Δ or magnetization of dopants M_z increases with the Cr-doping level in a monotonous manner, reaching a value of about 10 meV at $x = 0.21$ [Fig. 6(d)], comparable to the theoretical value [12]. In addition, there is nearly no difference between

samples of the same Cr-doping level but with different intrinsic doping or chemical potential. The error bar results from the local inhomogeneity in Cr doping.

To conclude, the zero-mode deviation demonstrates the existence of a mass term for the Dirac fermions in a magnetic field both in the surface- and bulk-doping cases. Compared with the top-Sb-layer doping case where there seems no clear signature of mass acquisition at zero field, there is evidence of easier spontaneous perpendicular alignment of magnetic moments in Sb_2Te_3 films with bulk Cr doping ($x = 0.08$). In addition, the heavily Cr-doped ($x = 0.18$) Sb_2Te_3 layer is suggested to be still in the topologically nontrivial region. Thus the introducing of a mass term, the isovalent nature of doping, the robustness of nontrivial band topology against Cr doping, and the effect of Dirac energy lifting imply that the Cr-doped Sb_2Te_3 film is a potential candidate of realizing many exotic topological magnetoelectric phenomena.

ACKNOWLEDGMENTS

This work was financially supported by National Science Foundation and Ministry of Science and Technology of China. Y. P. Jiang was partly supported by the NSF-USA (Grant No. DMR-1104256).

[1] M. Z. Hasan and C. L. Kane, Rev. Mod. Phys. **82**, 3045 (2010).
[2] X.-L. Qi and S.-C. Zhang, Rev. Mod. Phys. **83**, 1057 (2011).
[3] A. M. Essin, J. E. Moore, and D. Vanderbilt, Phys. Rev. Lett. **102**, 146805 (2009).
[4] K. Nomura and N. Nagaosa, Phys. Rev. Lett. **106**, 166802 (2011).
[5] X.-L. Qi, T. L. Hughes, and S.-C. Zhang, Phys. Rev. B **78**, 195424 (2008).
[6] X.-L. Qi, R. Li, J. Zang, and S.-C. Zhang, Science **323**, 1184 (2009).
[7] C.-Z. Chang, J. Zhang, X. Feng, J. Shen, Z. Zhang, M. Guo, K. Li, Y. Ou, P. Wei, L.-L. Wang, Z.-Q. Ji, Y. Feng, S. Ji, X. Chen, J. Jia, X. Dai, Z. Fang, S.-C. Zhang, K. He, Y. Wang, L. Lu, X.-C. Ma, and Q.-K. Xue, Science **340**, 167 (2013).
[8] R. Yu, W. Zhang, H.-J. Zhang, S.-C. Zhang, X. Dai, and Z. Fang, Science **329**, 61 (2010).
[9] Y. L. Chen, J. G. Analytis, J.-H. Chu, Z. K. Liu, S.-K. Mo, X. L. Qi, H. J. Zhang, D. H. Lu, X. Dai, Z. Fang, S. C. Zhang, I. R. Fisher, Z. Hussain, and Z.-X. Shen, Science **325**, 178 (2009).
[10] Y. Xia, D. Qian, D. Hsieh, L. Wray, A. Pal, H. Lin, A. Bansil, D. Grauer, Y. S. Hor, R. J. Cava, and M. Z. Hasan, Nat. Phys. **5**, 398 (2009).
[11] H. Zhang, C.-X. Liu, X.-L. Qi, X. Dai, Z. Fang, and S.-C. Zhang, Nat. Phys. **5**, 438 (2009).
[12] D. A. Abanin and D. A. Pesin, Phys. Rev. Lett. **106**, 136802 (2011).
[13] C.-Z. Chang, J. Zhang, M. Liu, Z. Zhang, X. Feng, K. Li, L.-L. Wang, X. Chen, X. Dai, Z. Fang, X.-L. Qi, S.-C. Zhang, Y. Wang, K. He, X.-C. Ma, and Q.-K. Xue, Adv. Mater. **25**, 1065 (2013).
[14] Q. Liu, C.-X. Liu, C. Xu, X.-L. Qi, and S.-C. Zhang, Phys. Rev. Lett. **102**, 156603 (2009).
[15] J.-J. Zhu, D.-X. Yao, S.-C. Zhang, and K. Chang, Phys. Rev. Lett. **106**, 097201 (2011).
[16] J. Zhang, C.-Z. Chang, P. Tang, Z. Zhang, X. Feng, K. Li, L.-l. Wang, X. Chen, C. Liu, W. Duan, K. He, Q.-K. Xue, X. Ma, and Y. Wang, Science **339**, 1582 (2013).
[17] J. G. Checkelsky, J. Ye, Y. Onose, Y. Iwasa, and Y. Tokura, Nat. Phys. **8**, 729 (2012).
[18] Y. L. Chen, J.-H. Chu, J. G. Analytis, Z. K. Liu, K. Igarashi, H.-H. Kuo, X. L. Qi, S. K. Mo, R. G. Moore, D. H. Lu, M. Hashimoto, T. Sasagawa, S. C. Zhang, I. R. Fisher, Z. Hussain, and Z. X. Shen, Science **329**, 659 (2010).
[19] C.-Z. Chang, P. Tang, Y.-L. Wang, X. Feng, K. Li, Z. Zhang, Y. Wang, L.-L. Wang, X. Chen, C. Liu, W. Duan, K. He, X.-C. Ma, and Q.-K. Xue, Phys. Rev. Lett. **112**, 056801 (2014).
[20] A. I. Figueroa, G. van der Laan, L. J. Collins-McIntyre, S. L. Zhang, A. A. Baker, S. E. Harrison, P. Schönherr, G. Cibin, and T. Hesjedal, Phys. Rev. B **90**, 134402 (2014).
[21] X. Kou, M. Lang, Y. Fan, Y. Jiang, T. Nie, J. Zhang, W. Jiang, Y. Wang, Y. Yao, L. He, and K. L. Wang, ACS Nano **7**, 9205 (2013).
[22] I. Lee, C. K. Kim, J. Lee, S. J. L. Billinge, R. Zhong, J. A. Schneeloch, T. Liu, T. Valla, J. M. Tranquada, G. Gu, and J. C. S. Davis, Proc. Natl. Acad. Sci. USA **112**, 1316 (2015).
[23] T. Sato, K. Segawa, K. Kosaka, S. Souma, K. Nakayama, K. Eto, T. Minami, Y. Ando, and T. Takahashi, Nat. Phys. **7**, 840 (2011).
[24] F. Yang, Y. R. Song, H. Li, K. F. Zhang, X. Yao, C. Liu, D. Qian, C. L. Gao, and J.-F. Jia, Phys. Rev. Lett. **111**, 176802 (2013).
[25] J.-M. Zhang, W. Ming, Z. Huang, G.-B. Liu, X. Kou, Y. Fan, K. L. Wang, and Y. Yao, Phys. Rev. B **88**, 235131 (2013).
[26] M. Bianchi, R. C. Hatch, J. Mi, B. B. Iversen, and P. Hofmann, Phys. Rev. Lett. **107**, 086802 (2011).
[27] Y. Jiang, Y. Wang, M. Chen, Z. Li, C. Song, K. He, L. Wang, X. Chen, X. Ma, and Q.-K. Xue, Phys. Rev. Lett. **108**, 016401 (2012).
[28] M. R. Scholz, J. Sánchez-Barriga, D. Marchenko, A. Varykhalov, A. Volykhov, L. V. Yashina, and O. Rader, Phys. Rev. Lett. **108**, 256810 (2012).
[29] T. Valla, Z. H. Pan, D. Gardner, Y. S. Lee, and S. Chu, Phys. Rev. Lett. **108**, 117601 (2012).
[30] L. A. Wray, S.-Y. Xu, Y. Xia, D. Hsieh, A. V. Fedorov, Y. S. Hor, R. J. Cava, A. Bansil, H. Lin, and M. Z. Hasan, Nat. Phys. **7**, 32 (2011).
[31] S.-Y. Xu, M. Neupane, C. Liu, D. Zhang, A. Richardella, L. Andrew Wray, N. Alidoust, M. Leandersson, T. Balasubramanian, J. Sanchez-Barriga, O. Rader, G. Landolt, B. Slomski, J. Hugo Dil, J. Osterwalder, T.-R. Chang, H.-T. Jeng, H. Lin, A. Bansil, N. Samarth, and M. Zahid Hasan, Nat. Phys. **8**, 616 (2012).
[32] Y. Zhang, K. He, C.-Z. Chang, C.-L. Song, L.-L. Wang, X. Chen, J.-F. Jia, Z. Fang, X. Dai, W.-Y. Shan, S.-Q. Shen, Q. Niu, X.-L. Qi, S.-C. Zhang, X.-C. Ma, and Q.-K. Xue, Nat. Phys. **6**, 584 (2010).
[33] P. Cheng, C. Song, T. Zhang, Y. Zhang, Y. Wang, J.-F. Jia, J. Wang, Y. Wang, B.-F. Zhu, X. Chen, X. Ma, K. He, L. Wang,

X. Dai, Z. Fang, X. Xie, X.-L. Qi, C.-X. Liu, S.-C. Zhang, and Q.-K. Xue, Phys. Rev. Lett. **105**, 076801 (2010).
[34] T. Hanaguri, K. Igarashi, M. Kawamura, H. Takagi, and T. Sasagawa, Phys. Rev. B **82**, 081305 (2010).
[35] Y. Okada, M. Serbyn, H. Lin, D. Walkup, W. Zhou, C. Dhital, M. Neupane, S. Xu, Y. J. Wang, R. Sankar, F. Chou, A. Bansil, M. Z. Hasan, S. D. Wilson, L. Fu, and V. Madhavan, Science **341**, 1496 (2013).
[36] Y. Okada, W. Zhou, C. Dhital, D. Walkup, Y. Ran, Z. Wang, S. D. Wilson, and V. Madhavan, Phys. Rev. Lett. **109**, 166407 (2012).
[37] Y. Zhang, Y.-W. Tan, H. L. Stormer, and P. Kim, Nature (London) **438**, 201 (2005).
[38] G. P. Mikitik and Y. V. Sharlai, Phys. Rev. Lett. **82**, 2147 (1999).
[39] H.-Z. Lu, J. Shi, and S.-Q. Shen, Phys. Rev. Lett. **107**, 076801 (2011).
[40] A. A. Taskin and Y. Ando, Phys. Rev. B **84**, 035301 (2011).
[41] C.-X. Liu, X.-L. Qi, H. J. Zhang, X. Dai, Z. Fang, and S.-C. Zhang, Phys. Rev. B **82**, 045122 (2010).
[42] Y. Jiang, Y. Y. Sun, M. Chen, Y. Wang, Z. Li, C. Song, K. He, L. Wang, X. Chen, Q.-K. Xue, X. Ma, and S. B. Zhang, Phys. Rev. Lett. **108**, 066809 (2012).
[43] Y.-S. Fu, M. Kawamura, K. Igarashi, H. Takagi, T. Hanaguri, and T. Sasagawa, Nat. Phys. **10**, 815 (2014).
[44] Z. Zhou, Y.-J. Chien, and C. Uher, Phys. Rev. B **74**, 224418 (2006).
[45] C. Niu, Y. Dai, Y. Zhu, Y. Ma, L. Yu, S. Han, and B. Huang, Sci. Rep. **2**, 976 (2012).
[46] J. Zhang, C.-Z. Chang, Z. Zhang, J. Wen, X. Feng, K. Li, M. Liu, K. He, L. Wang, X. Chen, Q.-K. Xue, X. Ma, and Y. Wang, Nat. Commun. **2**, 574 (2011).
[47] H. Jin, J.-H. Song, and A. J. Freeman, Phys. Rev. B **83**, 125319 (2011).
[48] M. Ye, S. V. Eremeev, K. Kuroda, M. Nakatake, S. Kim, Y. Yamada, E. E. Krasovskii, E. V. Chulkov, M. Arita, H. Miyahara, T. Maegawa, K. Okamoto, K. Miyamoto, T. Okuda, K. Shimada, H. Namatame, M. Taniguchi, Y. Ueda, and A. Kimura, arXiv:1112.5869.
[49] M. M. Vazifeh and M. Franz, Phys. Rev. B **86**, 045451 (2012).
[50] Y. Liu, Y. Y. Li, S. Rajput, D. Gilks, L. Lari, P. L. Galindo, M. Weinert, V. K. Lazarov, and L. Li, Nat. Phys. **10**, 294 (2014).
[51] I. Zeljkovic, Y. Okada, M. Serbyn, R. Sankar, D. Walkup, W. Zhou, J. Liu, G. Chang, Y. J. Wang, M. Z. Hasan, F. Chou, H. Lin, A. Bansil, L. Fu, and V. Madhavan, Nat. Mater. **14**, 318 (2015).
[52] R. R. Biswas and A. V. Balatsky, Phys. Rev. B **81**, 233405 (2010).